Journal of Solid State Chemistry **161,** 106–112 (2001)
doi:10.1006/jssc.2001.9295, available online at http://www.idealibrary.com on IDEAL®

The Influence of Composition and Temperature on the Phases in $Sr_{1-x}Ba_xZrO_3$ Perovskites: A High-Resolution Powder Diffraction Study

B. J. Kennedy

The Heavy Metals Research Centre, School of Chemistry, The University of Sydney, Sydney, New South Wales 2006, Australia

and

C. J. Howard, G. J. Thorogood, and J. R. Hester

Australian Nuclear Science and Technology Organisation, Private Mail Bag 1, Menai, New South Wales 2234, Australia

Received April 4, 2001; in revised form June 26, 2001; accepted July 2, 2001; published online August 22, 2001

High-resolution synchrotron X-ray diffraction measurements on a series of polycrystalline samples of $Sr_{1-x}Ba_xZrO_3$ at room temperature show that the symmetry increases with increasing Ba content, the sequence of phases being orthorhombic *Pnma*, orthorhombic *Imma*, tetragonal *I4/mcm*, and cubic *Pm*$\bar{3}$*m*. The effect of temperature has also been studied for a number of compositions and indicates that the same series of phases is present. The transition temperatures decrease with increasing Ba content. © 2001 Academic Press

INTRODUCTION

The diversity of structures exhibited by ABO_3 type perovskites continues to fascinate in a range of areas including solid state chemistry and physics and the earth sciences. While part of this fascination is curiosity driven, increasingly interest stems from the importance of perovskites in areas as diverse as magnetic and/or electronic devices and energy storage and transfer systems. Although the ideal perovskite structure is cubic, the potentially conflicting bonding requirements of the two cations often results in a lowering of symmetry. Indeed the mineral perovskite ($CaTiO_3$) itself has an orthorhombic structure under ambient conditions. There are two ways by which cubic symmetry can be observed in $CaTiO_3$-based perovskites, the first is by heating the sample (1) (or, ideally, decreasing the pressure) and the second is to optimize the ratio of the sizes of the *A* and *B* type cations by chemical substitution (2). Both approaches have been widely investigated for $CaTiO_3$ with early studies often in disagreement, presumably due to the high degree of pseudosymmetry in these systems (1–6). It is now accepted that heating $CaTiO_3$ results in transition to the cubic ($Pm\bar{3}m$) structure around 1580 K, via a tetragonal ($I4/mcm$) intermediate (1, 3, 4). There is speculation in the literature that a second orthorhombic intermediate phase is also involved (1, 3). Doping $CaTiO_3$ with Sr, forming $Ca_{1-x}Sr_xTiO_3$, results in a transformation to cubic at around $x = 0.9$ (2). Again there is a well-characterized tetragonal phase and the suggestion of a second intermediate phase (2, 3). Our very recent electron diffraction studies demonstrated that $Ca_{0.5}Sr_{0.5}TiO_3$ has *Pnma*, not the postulated *Cmcm*, symmetry but the existence and space group of any intermediate orthorhombic phase in this series remains unresolved (7).

By comparison with the intense interest in $CaTiO_3$ and its various substituted analogs the related zirconates have received very little attention. This is somewhat surprising since $SrZrO_3$ provided the first definitive evidence for any intermediate phase in the thermally induced $Pnma \rightarrow Pm\bar{3}m$ transition (8, 9). Although it was long believed that the sequence of the phases in $SrZrO_3$ was $Pnma \rightarrow Cmcm \rightarrow I4/mcm \rightarrow Pm\bar{3}m$ (9), very high resolution powder neutron diffraction studies have demonstrated that the intermediate orthorhombic phase is actually in *Imma*, and the sequence is in fact $Pnma \rightarrow Imma \rightarrow I4/mcm \rightarrow Pm\bar{3}m$ (10). The *Imma* space group (SG) has been considered "rare" in simple ABO_3 perovskites (11); however, increasing use of very high resolution diffractometers has resulted in a number of observations of this space group (12–14). There have been two recent studies of doped zirconates, $SrZr_{1-x}Ti_xO_3$ (15) and $BaZr_{1-x}Ce_xO_3$ (16). In both cases *B* type substitution has resulted in broadening of the diffraction peaks, precluding identification of the symmetry of any intermediate phase other than the ubiquitous tetragonal $I4/mcm$, phase (15, 16).

0022-4596/01 $35.00

In the current work we present results from a synchrotron diffraction study of the $Sr_{1-x}Ba_xZrO_3$ system. In this system the end-members have orthorhombic ($SrZrO_3$ SG *Pnma*) and cubic ($BaZrO_3$ SG $Pm\bar{3}m$) symmetry. This suggests it should be possible to stabilize intermediate structures by suitable substitutions. Equally importantly, by analogy with the well-studied $Ca_{1-x}Sr_xTiO_3$ system, it was thought likely that the substitution of the *A* type cation will result in minimal peak broadening in the diffraction patterns from intermediate compositions.

EXPERIMENTAL

Sample preparation

Approximately 20 g of each sample in the series $Sr_{1-x}Ba_xZrO_3$, where $x = 0$, 0.1, 0.2, 0.3, 0.35, 0.4, 0.45, 0.5, 0.55, 0.6, 0.65, 0.7, 0.8, 0.9, and 1, were prepared as follows. Tetrabutylzirconate was dissolved in ethanol and then the solution was hydrolyzed with a water solution containing the appropriate amounts of $Sr(NO_3)_2$ and $Ba(NO_3)_2$. The combined solutions were shear mixed for 5 min and then dried at 90°C. The dried samples were placed into covered alumina crucibles and then calcined in air at 750°C for 1 h. The calcined samples were ball milled in water for 16 h and then dried again at 90°C. Once dry the powders were pelletized into 25-mm-diameter discs at 5 tonne. The samples were sintered at 1200°C for 40 h in air, then ground to provide samples for the X-ray work.

Instrumentation

High-resolution synchrotron X-ray diffraction patterns were recorded using the 530-mm Debye–Scherrer diffractometer on Beamline 20B (The ANBF) at the Photon Factory, Tsukuba (17). This instrument uses image plates (IP) as detectors, each Fuji 20×40-cm IP covering a 2θ angular range of 40°. The data are collected in 0.01° angular steps. Up to 25 diffraction patterns are recorded on each IP before removing it from the diffractometer. Room temperature patterns were initially recorded for all samples at $\lambda = 0.772$ Å, this being just below the Sr K edge. For these measurements the samples were housed in rotating 0.3-mm-diameter capillaries and data were collected using three IPs covering an angular range of 5–125°. Variable temperature measurements employed a custom-built furnace and were conducted at $\lambda = 0.995$ Å with the samples contained in rotating 0.5-mm-diameter quartz capillaries. In this case the data were collected using two IPs covering an angular range of 10–90°.

Structural Analysis

Structures were refined using the Rietveld method implemented in the program Rietica (18). In these analyses the data from the individual IPs were treated as separate histograms in the refinements, with the instrumental and profile parameters constrained to be equal for each histogram. In all cases the background of the lowest angle histogram was estimated by interpolation of up to 40 points and the background in the higher angle histograms was defined by a third-order polynomial in 2θ that was refined simultaneously with the other profile parameters. A number of the samples contained a small amount of baddeleyite (monoclinic ZrO_2) and this was included as a second phase in the structural refinements.

RESULTS AND DISCUSSION

Room Temperature Structures

The powder diffraction patterns over selected angular ranges from some representative examples of the $Sr_{1-x}Ba_xZrO_3$ series are shown in Figs. 1–3. As expected from the relative size of the Sr^{2+} and Ba^{2+} cations there is a systematic shift of the peaks to lower angles upon incorporation of the larger Ba^{2+} ion. Examination of the individual patterns rapidly confirmed that the sample of $SrZrO_3$ had the expected orthorhombic (*Pnma*) symmetry and $BaZrO_3$ had cubic ($Pm\bar{3}m$) symmetry. The BO_6 octahedra in perovskites in *Pnma* have two tilts ($a^+b^-b^-$ in Glazer's notation (19)), and the diffraction patterns show characteristic *R*-point reflections due to octahedra in successive layers tilting in the opposite sense (out-of-phase or $-$ tilts) and *M*-point reflections due to the octahedra in successive layers tilting in the same sense (in-phase or $+$ tilts). There are no tilts in the cubic structure ($a^\circ a^\circ a^\circ$) $Pm\bar{3}m$. As noted

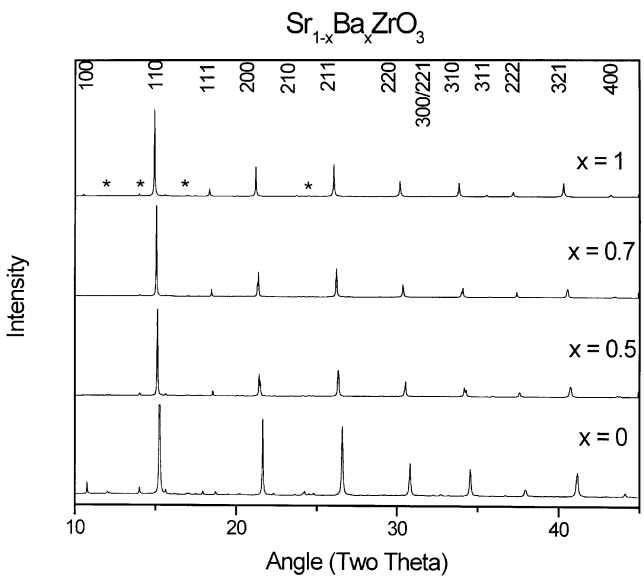

FIG. 1. Powder X-ray diffraction patterns for representative members of the series $Sr_{1-x}Ba_xZrO_3$ in the region 10–45° recorded at $\lambda = 0.7$ Å. The reflection indices shown are for the cubic ($x = 1$) phase. Peaks due to ZrO_2 are indicated by asterisks.

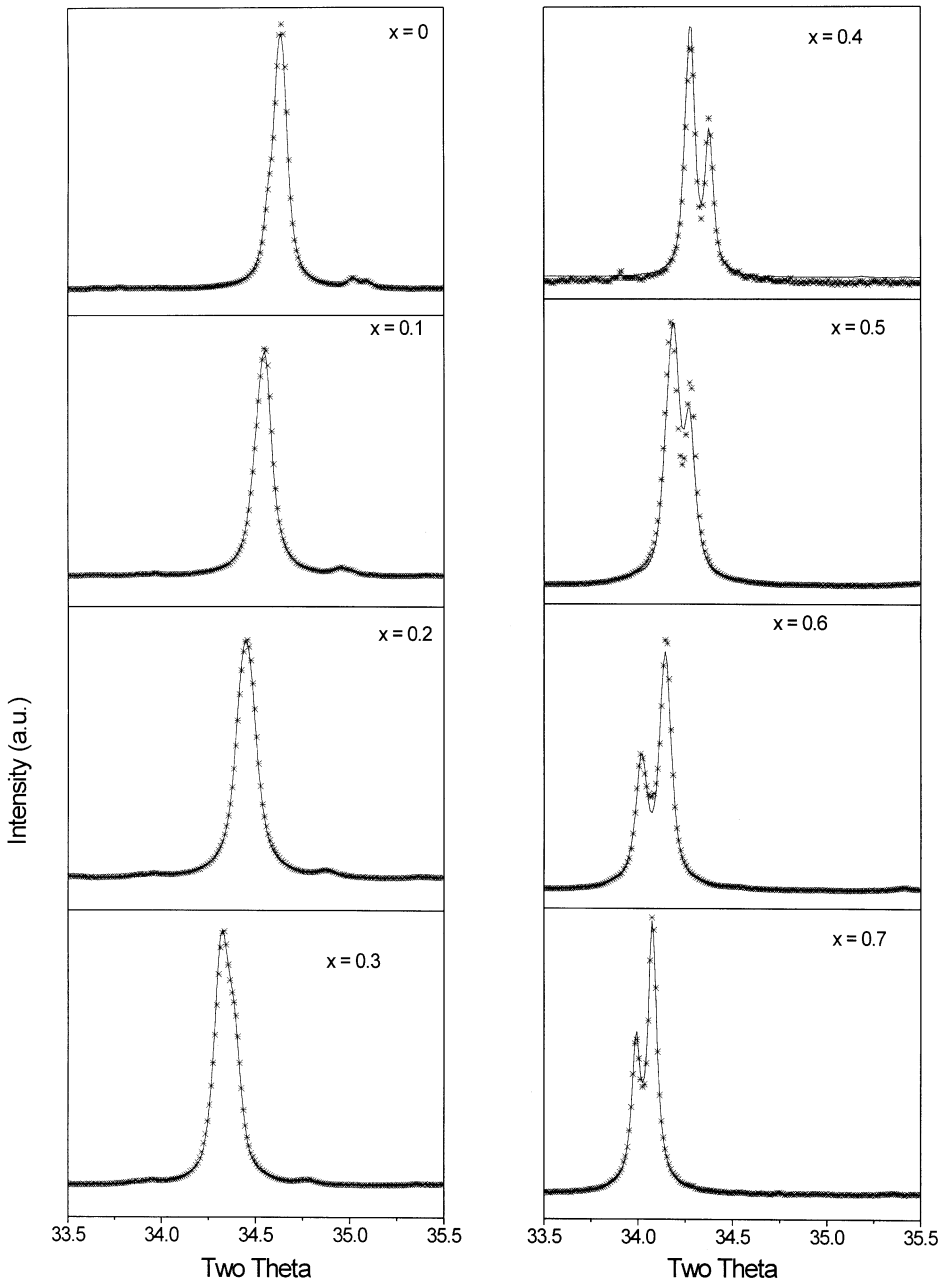

FIG. 2. Region of the powder diffraction patterns showing the (cubic) 310 reflection for selected compositions in the series $Sr_{1-x}Ba_xZrO_3$. In all cases the symbols are the observed data and the solid lines were calculated using the Rietveld method and the space groups listed in Table 1. The figure shows the reversal of the two reflections between $x = 0.5$ and 0.6. Note also the progressive shift of the reflections to lower angles with increasing content of the larger Ba cations.

previously, identification of the correct space group for perovskites can be far from trivial. In general we established the symmetry of the intermediate compounds based on the observation of resolved splitting or asymmetry in the appropriate reflections and/or the observation of the weak superlattice reflections that are diagnostic of the space group. In the present compounds the extremely strong X-ray scattering power of the heavy Ba and Zr atoms often made it difficult to detect those weak superlattice reflections that arise from displacement of the light O atoms even with the high signal-to-noise-ratio afforded by the diffractometer used. Consequently we placed greater than usual reliance on peak splitting to identify the appropriate symmetry. In all cases the structures were assigned the highest possible symmetry that fully accounted for the observed data (Table 1).

For each of the 15 compositions studied, from a combination of resolved peak splitting and the presence or absence

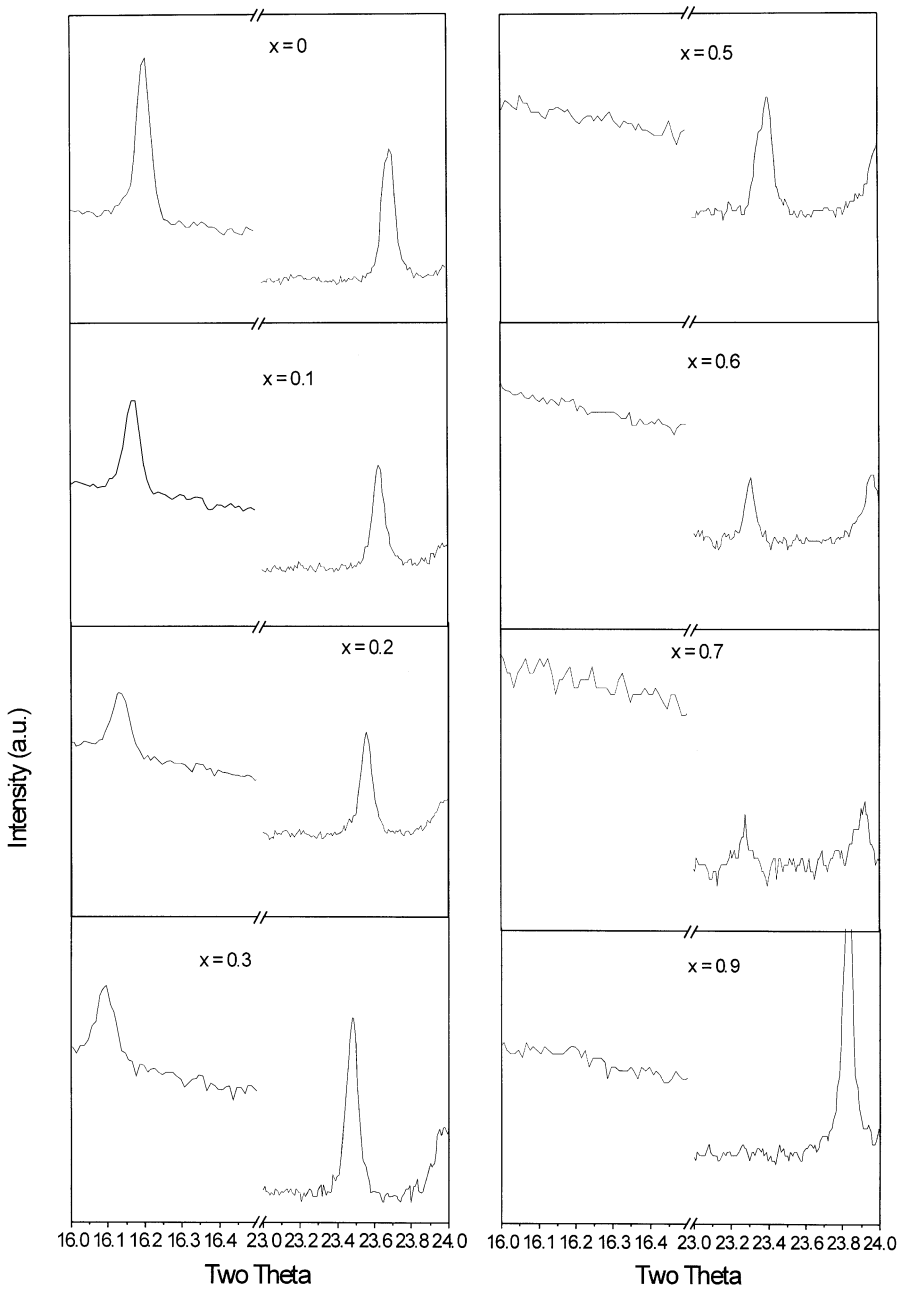

FIG. 3. Portions of the powder diffraction patterns for selected compositions in the series $Sr_{1-x}Ba_xZrO_3$. The M-point 210 reflection near $2\theta = 16.2^\circ$ shows the existence of in-phase tilts of the BO_6 octahedra and the R-point 123 reflection near $2\theta = 23.5^\circ$ out-of-phase tilts. The M-point reflection is not observed for $x > 0.4$, nor is the R-point reflection for $x > 0.8$. Note that both the $x = 0.5$ and 0.6 samples show only R-point reflections. The higher background near $2\theta = 16^\circ$ is a consequence of scatter from the capillary.

of the strongest M-point and R-point reflections, the 021 near $2\theta = 16.2^\circ$ ($d = 2.75$ Å) and 123 near $2\theta = 23.5^\circ$ ($d = 1.92$ Å), respectively, we deduced the following symmetry limits: $0 \leq x \leq 0.50$, orthorhombic; $0.60 \leq x \leq 0.80$, tetragonal; and $0.90 \leq x \leq 1$, cubic. There appears to be a two-phase region near $x = 0.55$. The refinements in both the cubic and the tetragonal regions were unexceptional, in all cases through the combination of narrow capillaries and high energies (short λ) physically reasonable atomic displacement parameters (ADP) were obtained for all atoms, including the light oxygen atoms. Considering the Sr-rich compounds $x \leq 0.4$, similarly satisfactory refinements were obtained, using SG *Pnma*, as judged by the measures of fit, physically reasonable bond distances, and ADP. At intermediate Sr levels the patterns were not well fitted in *Pnma*, in that this model calculated intensity near

TABLE 1
Refined Cell Parameters, Cell Volumes, and Space Groups of $Sr_{1-x}Ba_xZrO_3$ ($0 \leq x \leq 1$) at Room Temperature

x	a(Å)	b(Å)	c(Å)	Cell volume (Å^3)	Space group
0.00	5.81793(6)	8.20386(8)	5.79386(5)	276.538(5)	*Pnma*
0.10	5.8281(1)	8.2230(2)	5.8116(1)	278.520(9)	*Pnma*
0.20	5.8355(1)	8.2338(2)	5.8256(1)	279.911(10)	*Pnma*
0.30	5.8532(4)	8.2579(1)	5.8518(3)	282.844(25)	*Pnma*
0.35	5.8568(1)	8.2631(1)	5.8604(1)	283.615(8)	*Pnma*
0.40	5.8727(2)	8.2715(2)	5.8650(2)	284.896(14)	*Pnma*
0.45	5.87042(6)	8.27766(8)	5.88047(6)	285.752(5)	*Imma*
0.50	5.86860(4)	8.28670(12)	5.88451(8)	286.171(6)	*Imma*
0.55	Two phase				*Imma-I4/mcm*
0.60	5.88164(4)		8.35285(6)	288.956(3)	*I4/mcm*
0.65	5.88885(3)		8.35974(5)	289.903(3)	*I4/mcm*
0.70	5.89577(3)		8.36214(3)	290.669(3)	*I4/mcm*
0.80	5.9225(1)		8.3669(2)	293.48(1)	*I4/mcm*
0.90	4.18916(4)			73.516(1)	$Pm\bar{3}m$
1.00	4.19466(2)			73.805(1)	$Pm\bar{3}m$

Note. The numbers in parentheses are the estimated standard deviations.

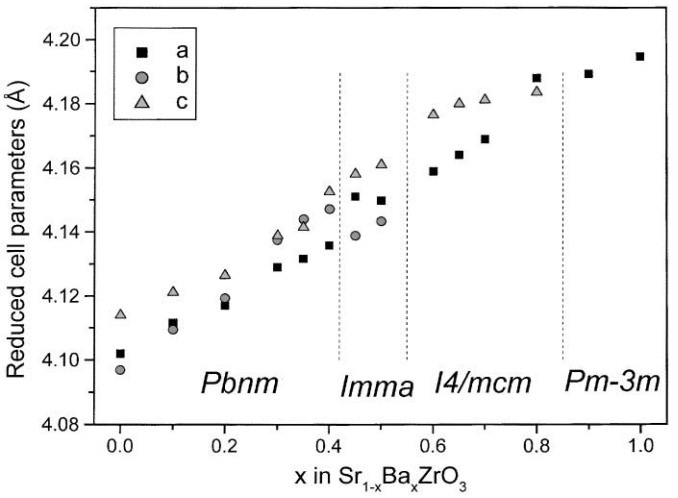

FIG. 4. Reduced cell parameters plotted as a function of x in the $Sr_{1-x}Ba_xZrO_3$ system at room temperature.

$d = 2.75$ Å where none was observed and yet the tetragonal $I4/mcm$ ($a^\circ a^\circ c^-$) model also proved unsatisfactory. As a consequence of both the weak intensity of the superlattice reflections, arising from the tilting of the ZrO_6 octahedra, and the presence in the samples of trace amounts of ZrO_2, identification of the correct space groups from first principles was not feasible. Rather we relied on recent group theoretical (20) and powder neutron diffraction studies on $SrZrO_3$ (10) to identify possible space groups.

As discussed recently by Howard and Stokes (20) it is not possible for an ABO_3 perovskite to undergo a continuous transition from *Pnma* to *I4/mcm*. However perovskites in *Pnma* can continuously transform to a number of higher symmetry structures, just as *I4/mcm* can continuously transform to (different) low symmetry analogs. In our recent neutron diffraction study of $SrZrO_3$, which employed fine temperature intervals, we observed the loss of the *M*-point reflections indicative of in-phase rotations of the ZrO_6 octahedra well before the first-order transition to the tetragonal *I4/mcm* structure. This together with the observed reversal of the apparent tetragonal splitting from $c/a < 1$ to $c/a > 1$ *and* Rietveld refinements led to the conclusion that the space group for the intermediate phase was *Imma* (10).

In the present case the composition steps are comparatively coarse. Nevertheless, the same phenomena appear; that is, the *M*-point reflections are no longer observed at Ba contents greater than $x = 0.45$ and this is before the onset of the first-order phase transition to *I4/mcm* near $x = 0.60$. Further there is a reversal of the pseudotetragonal c/a ratio at around $x = 0.55$. The intermediate orthorhombic phase is clearly not *Cmcm*, as that would give rise to both *R*-point and *M*-point reflections. By comparison with $SrZrO_3$ we conclude that the same *Imma* ($a^\circ b^- b^-$) intermediate phase is involved in the transition. The variation in the lattice parameters is shown in Fig. 4 and the apparently continuous transition from *Pnma* to *Imma* and the first-order transition from *Imma* to *I4/mcm* are consistent with the work of Howard and Stokes (20). In cases where the *M*-point reflections were difficult to observe the Rietveld refinements were unhelpful in distinguishing *Pnma* from *Imma*.

Variable Temperature Studies

The structures of five compositions were studied at elevated temperatures and in three cases, $x = 0.60$, 0.50, and 0.40, the transitions to cubic were observed. For $x = 0.35$ the transition to cubic appears to be just above 800°C, the highest temperature accessible in this study. For $x = 0.30$ the tetragonal structure was only observed near the maximum temperature available and the transition to cubic seemed remote. Where observed, the temperatures of both the transitions from orthorhombic to tetragonal and tetragonal to cubic decreased with increasing Ba content, thus mimicking the behavior at room temperature.

As evident from Fig. 4, in the tetragonal phase the temperature variation of the lattice parameters for all compositions display similar behavior, in that c is approximately constant whereas a increases rapidly as the temperature is increased. It can be seen in the case of the $x = 0.6$ sample that the reduced c parameter lies above the extrapolated value of the cubic lattice parameter and the reduced a parameter lies below this extrapolation in such a way that the cell volume varies essentially linearly with temperature. The shape of the curves in Fig. 5 is similar to that displayed by other well-characterized ABO_3 perovskites, including $SrZrO_3$ and $CaTiO_3$, and appears typical of a tricritical phase transition.

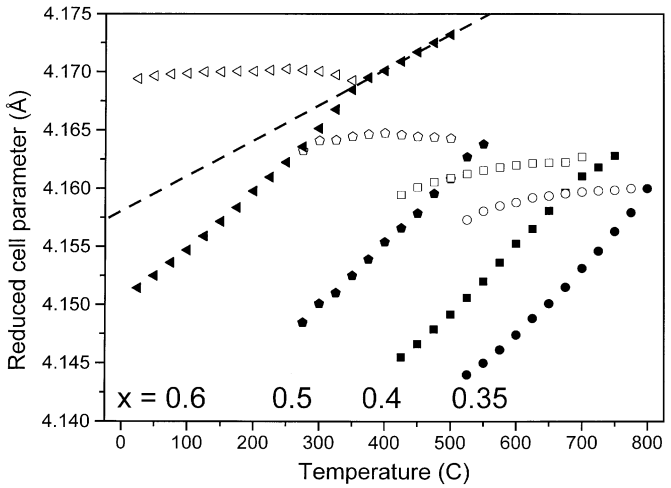

FIG. 5. Temperature dependence of the reduced cell parameters for the series $Sr_{1-x}Ba_xZrO_3$, $x = 0.35$, 0.4, 0.5, and 0.6. In all cases the data were collected from room temperature to the highest indicated temperature; however, for clarity only values in the tetragonal region are included. The dotted line for the $x = 0.6$ sample is the linear extrapolation from the values for the high-temperature cubic phase.

As explained above, the room temperature structure for the Sr-rich compounds with $x \leq 0.40$ is orthorhombic in *Pnma* based on the observation of both *M*-point and *R*-point reflections. Examination of the profiles for the $x = 0.40$ sample demonstrated this model to be satisfactory for patterns recorded up to 200°C. For patterns recorded above 400°C the patterns were clearly tetragonal with $c/a > 1$ (Fig. 6) and satisfactory fits were obtained in the tetragonal space group *I*4/*mcm*. Two features are apparent in the intermediate temperature region: first, between 200 and 300°C the patterns appear to be tetragonal but with $c/a < 1$ and, just above this, at 350°C, a more complex pattern is observed which simplifies again to a tetragonal cell with $c/a > 1$. This apparent reversal of c/a is the same as that observed for the composition dependence described above and is taken as evidence for the presence of an *Imma* phase. Accordingly we have fitted the patterns between 200 and 300°C in *Imma*. The more complex patterns observed between 325 and 400°C occur as a result of the coexistence of the *Imma* and *I*4/*mcm* phases and is consistent with the first-order transition linking these. Above 750°C the structure appears to be cubic since there is no evidence for any of the superlattice reflections nor do any of the peaks show broadening or splitting.

The temperature-dependent profiles for $x = 0.35$ exhibit very similar behavior, i.e., a region well-fitted in *Pnma*, a pseudotetragonal region with $c/a < 1$ fitted in *Imma*, a two-phase *Imma*–*I*4/*mcm* region, and a tetragonal region. For the $x = 0.5$ sample the room temperature structure is in *Imma* and this becomes tetragonal near 275°C and finally cubic near 550°C. The $x = 0.6$ sample has a tetragonal structure at room temperature and this undergoes a single phase transition to cubic near 350°C.

Whereas it was relatively straightforward to detect the onset of both the *I*4/*mcm* structure, based on the reversal of the apparent c/a ratio, and the $Pm\bar{3}m$ structure, based on the absence of any apparent splitting in the *h*00 type reflections, it was more difficult to detect the transition between the *Imma* and *Pnma* phases. The observation of the *Imma* phase is dependent on the loss of all peaks due to *M*-point

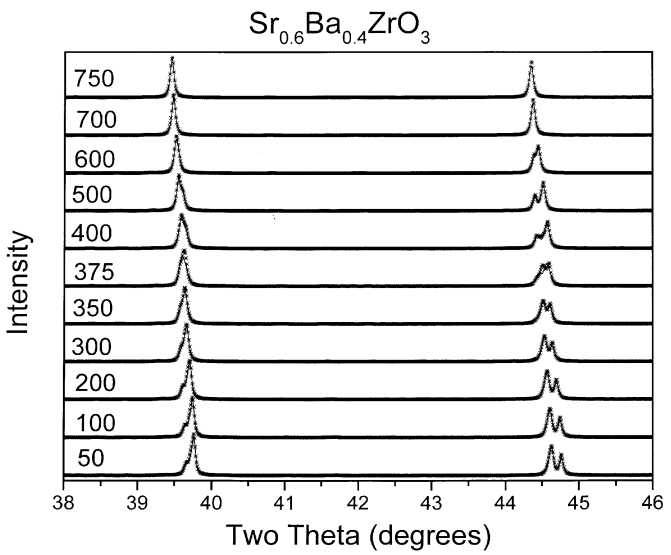

FIG. 6. Temperature dependence of portions of the powder diffraction patterns for $Sr_{0.6}Ba_{0.4}ZrO_3$ recorded at $\lambda = 1.0$ Å. In all cases the symbols are the observed data and the solid lines were calculated using the Rietveld method. The figure shows the reversal of the two reflections near 350°C.

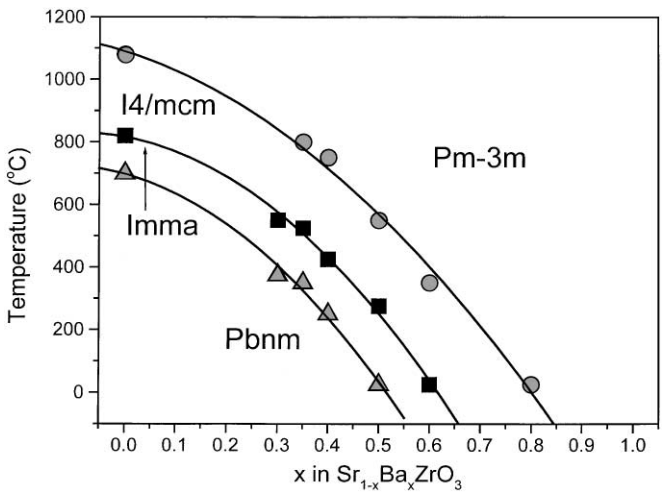

FIG. 7. Phase diagram of $Sr_{1-x}Ba_xZrO_3$ established from powder X-ray diffraction measurements.

distortions, prior to the first-order transition. The intensity of these peaks is extremely low ($< 1\%$ of the strongest reflection) and the higher absorption in the variable temperature measurements conducted at 1 Å is a disadvantage. The use of this longer wavelength is essential in detecting the $I4/mcm$–$Pm\bar{3}m$ transition. Nevertheless it appears that all compositions studied, except $x = 0.6$ which is tetragonal at room temperature, have an *Imma* phase, Fig. 7. This figure suggests that the *Imma* phase has limited existence at all Ba contents, although it is possible that it may not exist for compounds with Ba contents $x > 0.8$. No suitable cryostat was available for studies of this section of the phase diagram.

It is clear that the systematic variation of temperature and composition enables a fuller understanding of the structures of these apparently simple oxides. There is ample evidence from this and previous studies that chemical substitutions are a good mimic of temperature, provided that phase sequences of the end-members are expected to be similar. There is some merit in more extensive studies of systems with conflicting structural pathways as occurs in the $LaCrO_3$–$SrTiO_3$ system (21). The existence of extensive two-phase regions in these apparently highly crystalline samples is somewhat surprising but is consistent with a first-order phase transition.

ACKNOWLEDGMENTS

This work was performed at the Australian National Beamline Facility with support from the Australian Synchrotron Research Program, which is funded by the Commonwealth of Australia under the Major National Research Facilities Program. B.J.K. acknowledges the support of the Australian Research Council.

REFERENCES

1. B. J. Kennedy, C. J. Howard, and B. C. Chakoumakos, *J. Phys.: Condens. Matter* **11,** 1479 (1999).
2. C. J. Ball, B. D. Begg, D. J. Cookson, G. J. Thorogood, and E. R. Vance, *J. Solid State Chem.* **139,** 238 (1998).
3. S. Qin, A. I. Becerro, F. Seifert, J. Gottsmann, and J. Jiang, *J. Mater.* **10,** 1609 (2000).
4. S. A. T. Redfern, *J. Phys.: Condens. Matter* **8,** 8267 (1996).
5. T. Vogt and W. W. Schmahl, *Europhys. Lett.* **24,** 281 (1993).
6. R. Ranjan, D. Pandey, V. Siruguri, P. S. Krishna, and S. K. Paranjpe, *J. Phys.: Condens. Matter* **11,** 2233 (1999).
7. C. J. Howard, R. L. Withers, and B. J. Kennedy, *J. Solid State Chem.* **160,** 8 (2001).
8. L. Carlsson, *Acta Crystallogr.* **23,** 901 (1967).
9. M. Ahtee, A. M. Glazer, and A. W. Hewat, *Acta Crystallogr. B* **34,** 752 (1976).
10. C. J. Howard, K. S. Knight, E. H. Kisi, and B. J. Kennedy, *J. Phys.: Condens. Matter* **12,** L677 (2000).
11. P. M. Woodward, *Acta Crystallogr. B* **53,** 44 (1997).
12. S. Moussa, B. J. Kennedy, B. A. Hunter, and T. Vogt, *Solid State Commun.*, in press.
13. S. Moussa, B. J. Kennedy, B. A. Hunter, C. J. Howard, and T. Vogt, *J. Phys.: Condens. Matter* **13,** L203 (2001).
14. K. S. Knight, *Solid State Ionics* **74,** 109 (1994).
15. T. K-Y Wong, B. J. Kennedy, C. J. Howard, B. A. Hunter, and T. Vogt, *J. Solid State Chem.* **156,** 255 (2001).
16. I. Charrier-Cougoulic, T. Pagnier, and G. Lacazeau, *J. Solid State Chem.* **142,** 220 (1999).
17. T. M. Sabine, B. J. Kennedy, R. F. Garrett, G. J. Foran, and D. J. Cookson, *J. Appl. Crysallogr.* **28,** 513 (1995).
18. C. J. Howard and B. A. Hunter, A Computer Program for Rietveld Analysis of X-ray and Neutron Powder Diffraction Patterns, Lucas Heights Research Laboratories, pp. 1–27, 1998.
19. A. M. Glazer, *Acta Crystallogr. B* **28,** 3384 (1972).
20. C. J. Howard and H. T. Stokes, *Acta Crystallogr. B* **54,** 782 (1998).
21. B. J. Kennedy, C. J. Howard, G. J. Thorogood, M. A. T. Mestre, and J. R. Hester, *J. Solid State Chem.* **155,** 455 (2000).